

Free vibration of FG-GPLRC conical panel on elastic foundation

Arameh Eyvazian¹, Farayi Musharavati¹, Faris Tarlochan¹,
Abdolreza Pasharavesh², Dipen Kumar Rajak³, Mohammed Bakr Husain⁴ and Tron Nhan Tran^{*5,6}

¹Mechanical and Industrial Engineering Department, Qatar University, Doha, Qatar

²Mechanical Engineering Department, Sharif University of Technology, Tehran, Iran

³Department of Mechanical Engineering, Sandip Institute of Technology and Research Center, Nashik, India

⁴Department of Biological and Environmental Sciences, Qatar University, Doha, Qatar

⁵Division of Computational Mechatronic, Institute for Computational Science, Ton Duc Thang University, Ho Chi Minh City, Vietnam

⁶Faculty of Electrical & Electronics Engineering, Ton Duc Thang University, Ho Chi Minh City, Vietnam

(Received December 17, 2019, Revised January 24, 2020, Accepted February 4, 2020)

Abstract. Present research is aimed to investigate the free vibration behavior of functionally graded (FG) nanocomposite conical panel reinforced by graphene platelets (GPLs) on the elastic foundation. Winkler-Pasternak elastic foundation surrounds the mentioned shell. For each ply, graphaene platelets are randomly oriented and uniformly dispersed in an isotropic matrix. It is assumed that the Volume fraction of GPLs reinforcement could be different from layer to layer according to a functionally graded pattern. The effective elastic modulus of the conical panel is estimated according to the modified Halpin-Tsai rule in this manuscript. Cone is modeled based on the first order shear deformation theory (FSDT). Hamilton's principle and generalized differential quadrature (GDQ) approach are also used to derive and discrete the equations of motion. Some evaluations are provided to compare the natural frequencies between current study and some experimental and theoretical investigations. After validation of the accuracy of the present formulation and method, natural frequencies and the corresponding mode shapes of FG-GPLRC conical panel are developed for different parameters such as boundary conditions, GPLs volume fraction, types of functionally graded and elastic foundation coefficients.

Keywords: conical panel; graphene platelets; GDQM; nanocomposite; elastic foundation

1. Introduction

Graphene has been discovered as a carbon nanostructure and two-dimensional single-atom layer in 2004 (see Novoselov *et al.* 2004). Graphene has shown excellent thermal and electrical conductivity. Its manufacturing is more cost-effective compared to other nanostructures based on carbon, i.e. nanotube. Furthermore, superior mechanical properties of such structure have attracted the attention of scientists and researchers. In this regard, numerous articles illustrate the research of scientists to find the excellent specifications of graphene (Reddy *et al.* 2006, Scarpa *et al.* 2009, cadelano *et al.* 2009, zhang *et al.* 2011). In this paper, the potential of graphene as a suitable reinforcement for nanocomposites and its application in the vibration phenomenon will be investigated.

According to reports in the open literature, graphene has much higher stiffness than many industrial materials such as stainless steel. The Young's modulus of these nanostructures is reported about 1Tpa. The conduction capacity of graphene is known to be a prominent feature of these materials as it is higher than copper and silver. In addition, the scientists demonstrated that a slight increase in graphene content of the composite will significantly improve the mechanical, electrical, and thermal properties

of the composite structure (Rafiee *et al.* 2009, Zhao *et al.* 2010). Because of the flat surface of graphene compared to the geometry of carbon nanotubes, these nanostructures as nanofillers could have better interactions with the polymer matrix. The other unique features of these nanostructures can be studied in the open literature (Stankovich *et al.* 2006, Potts *et al.* 2011).

Some experimental studies demonstrate introducing graphene even to a small extent on nanocomposite structures has been shown to improve the vibrational characteristics. Rafiee *et al.* (2009) found the enhanced stiffness and strength due to adding 0.1 w.t.% (weight fraction) of graphene platelets, is equivalent to incorporation 1 w.t.% of carbon nanotubes (CNTs). Theoretical analyses showed that the introducing of graphene either in sheets or platelets forms will increase the natural frequency of the structure compared to the graphene-free structure. For instance, Song *et al.* (2017) reported that adding only 1.2 wt.% graphene will enhance the natural frequency of the rectangular plate by 160 %. Chandra *et al.* (2012) investigated the impact of different models of nanocomposite fabrication on their vibration characteristic and indicated the key role of graphene sheets dimensions in improving the natural frequency of the structure. However, it should be noted that, the weight fraction of graphene reinforcement agent cannot be increased arbitrarily because higher weight fraction of graphene nanofillers will results in unsightly results (Kulkarni *et al.* 2010).

*Corresponding author, Ph.D.
E-mail: trantronghan@tdtu.edu.vn

As embedded reinforcement, graphene can be classified in two classes: graphene sheets (GRC) and graphene platelets (GPLRC). In the first class, thermo-mechanical properties are obtained based on the modified micro-mechanical rule that is provided by the calculated information of molecular dynamics simulations. Changes in the weight fraction of graphene sheets are considered in the range 3-11 percent and both the reinforcement and matrix are supposed temperature-dependent. Studies on the vibrations of graphene-reinforced structures are well documented in the open literature. Wang *et al.* (2019a) implemented the hybrid Kantorovich-Galerkin method to study the free vibration of nanocomposite beam embedded with graphene sheets. In the mentioned problem, two dimensional elasticity based on the plane-stress is used to model each layer of the beam. Natural frequencies of a functionally graded GRC beams on a two parameter elastic foundation in thermal environment are obtained by Shen *et al.* (2017a). In another work, Shen *et al.* (2019a) investigated large amplitude free vibration of a graphene reinforced post-buckled beam with considering the geometrical nonlinearity based on the von Kármán type. Linear and nonlinear free vibration of FG-GRC plates with and without considering elastic foundation are analyzed by Shen *et al.* (2019b) and Shen *et al.* (2017b). In these papers it is assumed that the thermal environment affected the natural frequencies which can be obtained using two-step perturbation technique. Kiani (2018) examined the nonlinear vibration characteristics of FG-GRC plates in thermal environment implementing NURBS based isogeometric finite element method. Using the mentioned method this Author examined the post-buckling of a FG-GPLRC plate (Kiani and Mirzaei 2019). It is revealed that among the three types of functionally graded patterns (FG-X,U,O) for graphene sheets, FG-X pattern results in the highest natural frequency while the nonlinear to linear frequency factor is the lowest for the mentioned pattern. A few papers are available on the vibration response of FG-GRC shells. Shen *et al.* (2017c) and Shen *et al.* (2018) explored the vibration behavior of cylindrical panels and shells. Influences of graphene sheets weight fraction and piece-wise pattern on the fundamental frequency are studied.

In another novel class, graphene platelets are introduced as fillers in the matrix of the composite structure and such structure is briefly called GPLRC. In this model of reinforced composites, thermo-elastic properties can be obtained using the Halpin-Tsai micromechanical rule. The weight fraction of graphene platelets in this class is less than 1% and material properties are independent of the temperature. The major works on the vibration analysis of structures embedded with graphene platelets are introduced as follows. Kitipornchai *et al.* (2017) analyzed vibrational behavior of functionally graded porous GPLRC beams implementing Ritz technique. Furthermore, nonlinear vibration using the Ritz method are investigated for FG-GPLRC beams by Feng *et al.* (2017). Wang *et al.* (2019b) studied the dynamic response of a higher order composite beam with graphene platelets reinforcements under two concentrated successive moving masses. Because of the nature of such problem, a Hybrid Navier-Newmark method

is used to solve the equations of motion. Anirudh *et al.* (2019) conducted a comprehensive study on the bending, free vibration and buckling of FG-GPLRC deep arches. In their study, they used finite element approximation to obtain the response of relative equations based on the trigonometric refined arch theory. Using the Navier method, vibrations of graphene platelets based nanocomposites were assessed for the first time by Song *et al.* (2017). Zhao *et al.* (2017) developed a refined analytical method to calculate the natural frequency of FG-GPLRC trapezoidal plates. Free vibration of nanocomposite plates reinforced by graphene platelets with quadrilateral shapes are analyzed utilizing IMLS-Ritz by Gua *et al.* (2018). Refined Halpin-Tsai micromechanical rule was developed for the mentioned paper. Nonlinear forced (Gholami and Anari 2018) and free vibration (Gao *et al.* 2018) analysis of functionally graded rectangular plates are explored in the open literature. The variation differential quadrature approach are introduced by Gholami and Ansari (2019) to analyze the effects of functionally graded patterns on the natural frequency of GPLRC plates. Malekzadeh *et al.* (2018) used the conformal mapping technique and generalized differential quadrature method to investigate the natural frequencies of an eccentric annular plates. Also, in this paper, it is assumed that the plate is embedded with two piezoelectric layers under the closed circuit condition. Influences of piezoelectric layers and supersonic flow on the vibrational response of FG-GPLRC plates are studied by Saidi *et al.* (2019).

Dong *et al.* (2018a) and Dong *et al.* (2018b) indicated the nonlinear free vibration analysis of FG-GPLRC cylindrical shells. The effect of the initial stresses caused by the spinning motion on the shell natural frequency is outlined. Utilizing an analytical approach and applying a three dimensional elasticity theory, Liu *et al.* (2018) examined the free vibration of an initially stressed FG-GPLRC composite cylindrical shell. Wang *et al.* (2018) proposed Navier solution to obtain the natural frequency of doubly curved shallow nanocomposite shells reinforced with graphene platelets.

The free vibrations of isotropic (Civalek 2007), Sandwich (Rahmani *et al.* 2019) and composite (Civalek 2006, Javed *et al.* 2016) conical panels and shells are evaluated in the open literature; However, the free vibration study of graphene platelets-reinforced conical panel has not been addressed.

In this regard, the present work applied the FSDT shell hypothesis and modified Halpin-Tsai micromechanical rule to research the free vibration characteristics of FG-GPLRC conical panel. Moreover, the GDQ method is implemented to discrete the governing motion equations in the two dimensional panel domain into a system of algebraic equations. The natural frequencies of laminated graphene platelet reinforced-composite conical panels on the Winkler-Pasternak elastic foundation are tabulated. Also, various functionally graded patterns are considered for graphene reinforcements into the formulation. The influence of other parameters are investigated on the natural frequencies and mode shape for free vibration phenomena.

$$r(x) = x \sin(\beta) \quad (1)$$

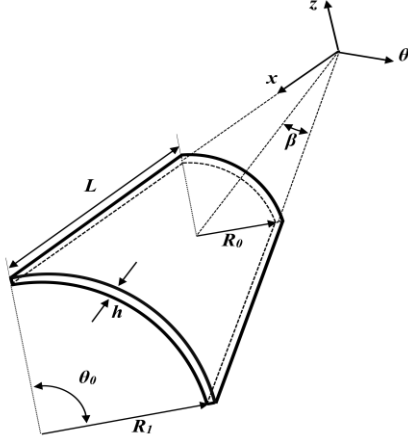


Fig. 1 Geometry of a conical panel.

2. Geometry and material properties of spherical shell

A functionally graded GPL conical panel of evenly thickness h , with angle of embrace θ_0 , finite length L , and vertex half angle β whose properties are graded along z direction is demonstrated in Figure (1). The coordinates along the meridional and circumferential directions are indicated by x and θ , respectively. Furthermore, z is measured from mid-surface across the thickness, positive outward. The radius of the shell at circumferential edges is equal to R_0, R_1 and the distance from each point to the axis of revolution is denoted by $r(x)$ which can be obtained using the following formula

In the present work, the laminated GPLRC conical panel is assumed to be completely bonded to each layer with the equal thickness. Each layer of the aforementioned composite consists of the combination of the isotropic matrix and graphene nanofillers which are uniformly and randomly embedded in the matrix. Therefore, the changes in the volume fraction of the platelets can be considered based on a step layer-wise model along the thickness.

The even number is selected for the number of layers N_L of the laminated composite structure. In order to distribute the nanoplatelets in the thickness direction, three functionally graded models can be used which are FG-O, FG-X, and UD. An isotropic and homogeneous shell can be modeled by choosing the uniform type (UD) model in which it is assumed that the volume fraction of graphene platelets is constant along the z direction. In the step functionally graded distributions, the GPL volume fraction linearly changes from ply to ply. For the case of X-GPLRC, the top and bottom layers are nanofillers rich while O-GPLRC indicates vice versa so that the middle layers are GPL-rich. Distribution of volume fraction for each layer is according to the following relation (see Wu *et al.* 2017)

$$U - \text{GPLRC} : V_{GPL}^{(k)} = V_{GPL}^*$$

$$X - \text{GPLRC} : V_{GPL}^{(k)} = 2V_{GPL}^*|2k - N_L - 1|/N_L \quad (2)$$

$$O - \text{GPLRC} : V_{GPL}^{(k)} = 2V_{GPL}^*(1 - |2k - N_L - 1|/N_L)$$

In the above relations, $V_{GPL}^{(k)}$ shows the volume fraction of platelets in the k -th layer of the composite. In Eq. (2) k varies from 1 to N_L . Also V_{GPL}^* denotes the total volume fraction of the GPLs in the conical panel and this parameter can be calculated in terms of the graphene platelets weight fraction W_{GPL} in the structure.

$$V_{GPL}^* = \frac{W_{GPL}}{W_{GPL} + \left(\frac{\rho_{GPL}}{\rho_m}\right)(1 - W_{GPL})} \quad (3)$$

ρ_{GPL} and ρ_m are mass density of the graphene platelets and isotropic matrix. Some researches has shown that the size and geometry of nanoplatelets are determining factors in the calculation of the mechanical properties of the composite. The micromechanical Halpin-Tsai rule is used to obtain the effective Young's modulus. This is a widely approved law in calculating the elasticity modulus of the composites that reinforced with graphene platelets (Affdl and Kardos 1976). Using this law, we can achieve the elasticity modulus of the composite structure by taking into the geometry and dimensions of the nanofillers in the following form:

$$E^{(k)} = \frac{3}{8} \frac{1 + \xi_L \eta_L V_{GPL}^{(k)}}{1 - \eta_L V_{GPL}^{(k)}} \times E_m + \frac{5}{8} \frac{1 + \xi_T \eta_T V_{GPL}^{(k)}}{1 - \eta_T V_{GPL}^{(k)}} \times E_m \quad (4)$$

where η_L and η_T are the auxiliary parameters expressed as

$$\eta_L = \frac{\left(\frac{E_{GPL}}{E_m}\right) - 1}{\left(\frac{E_{GPL}}{E_m}\right) + \xi_L}, \quad \eta_T = \frac{\left(\frac{E_{GPL}}{E_m}\right) - 1}{\left(\frac{E_{GPL}}{E_m}\right) + \xi_T} \quad (5)$$

In Eq. (5), E_m and E_{GPL} illustrate the Young's modulus of the isotropic matrix and GPLs, respectively. The geometrical factors of the platelets are determined in terms of the GPLs thickness, t_{GPL} , width, b_{GPL} and length, a_{GPL} as follows

$$\xi_L = 2 \left(\frac{a_{GPL}}{t_{GPL}}\right), \quad \xi_T = 2 \left(\frac{b_{GPL}}{t_{GPL}}\right) \quad (6)$$

The effective Poisson's ratio of the composite shell ν and The mass density of the composite shell ρ may be simply calculated utilizing the poisson's ratio and mass density of each constituents and deployment of the Voigt rule of mixtures. Accordingly one may write

$$\begin{aligned} \rho^{(k)} &= \rho_{GPL} V_{GPL}^{(k)} + \rho_m V_m^{(k)} \\ \nu^{(k)} &= \nu_{GPL} V_{GPL}^{(k)} + \nu_m V_m^{(k)} \end{aligned} \quad (7)$$

In Eq. (7), the subscripts m and GPL indicate the matrix and graphene platelets nanofiller, respectively. The volume fraction of polymer V_m can be obtain using this relation $V_m = 1 - V_{GPL}$.

3. Theoretical formulations

Love was the first researcher that presented a successful thin shell hypothesis based upon the classical linear

elasticity. This theory doesn't consider the shear deformation and rotary inertia. This theory is divided to two types. Firstly is named as the Love's first approximation and eliminates the thickness-to-radius ratio against the unit. Another one considers this ratio and is known as Low's second approximation. To apply the shear deformation effects along the thickness and rotary inertia influence, the first order shear deformation shell theory (FSDT) is implemented (Reddy 2006). Based on the FSDT, displacements field (u_1, u_2, u_3) of a supposed point in the conical panel domain are written as

$$\begin{aligned} u_1(x, \theta, z, t) &= u_1^0(x, \theta, t) + z\psi_1(x, \theta, t) \\ u_2(x, \theta, z, t) &= u_2^0(x, \theta, t) + z\psi_2(x, \theta, t) \\ u_3(x, \theta, z, t) &= u_3^0(x, \theta, t) \end{aligned} \quad (8)$$

where u_1^0 , u_2^0 , and u_3^0 are the displacements of the reference surface ($z = 0$) along the x , θ , and z directions, respectively. Moreover, ψ_1 and ψ_2 demonstrate the transverse normal rotations of the reference surface about the θ and x axes, respectively. t indicates the time variable.

Donnell propounded a simply hypothesis to use kinematic relations. This theory is most common for the shallow shells. Sanders developed novel relationships between strains and displacement components where are more appropriate for deep shells. In this research Sanders' theory are implemented to define the strain-displacement equations. According to the assumed theory, the in-plane strain components can be obtained using the linear functions of the thickness coordinate, while the out-of-plane shear strain components remain constant through the thickness. According to the given definitions, strains may be expressed in vector forms as (Reddy 2006)

$$\{\varepsilon\} = \{\varepsilon^0\} + z\{\varepsilon^1\} \quad (9)$$

where

$$\begin{Bmatrix} \varepsilon_1^0 \\ \varepsilon_2^0 \\ \varepsilon_4^0 \\ \varepsilon_5^0 \\ \varepsilon_6^0 \end{Bmatrix} = \begin{Bmatrix} u_{1,x}^0 \\ \frac{1}{r(x)}(u_{2,\theta}^0 + \sin(\beta)u_1^0 + \cos(\beta)u_3^0) \\ \frac{1}{r(x)}u_{3,\theta}^0 - \frac{\cos(\beta)}{r(x)}u_2^0 + \psi_2 \\ u_{3,x}^0 + \psi_1 \\ u_{2,x}^0 + \frac{1}{r(x)}(u_{1,\theta}^0 - \sin(\beta)u_2^0) \end{Bmatrix} \quad (10)$$

$$\begin{Bmatrix} \varepsilon_1^1 \\ \varepsilon_2^1 \\ \varepsilon_4^1 \\ \varepsilon_5^1 \\ \varepsilon_6^1 \end{Bmatrix} = \begin{Bmatrix} \psi_{1,x} \\ \frac{1}{r(x)}(\psi_{2,\theta} + \sin(\beta)\psi_1) \\ 0 \\ 0 \\ \psi_{2,x} + \frac{1}{r(x)}(\psi_{1,\theta} - \sin(\beta)\psi_2) \end{Bmatrix} \quad (11)$$

in which ε_1^0 , ε_2^0 , and ε_6^0 are the membrane strains of the middle surface; ε_1^1 , ε_2^1 , and ε_6^1 indicate the curvature variations of the conical panel; ε_4^0 , ε_5^0 are the transverse

shear strains. It is worth nothing that vanishing the $-\frac{\cos(\beta)}{r(x)}u_2^0$ term from the Eq. (10) converts the Sanders to Donnell theory.

In the present work, the materials are considered elastic and linear; therefore, the constitutive law for every layer of the FG-GPLRC conical panel can be obtained based on the Hook's law

$$\begin{Bmatrix} \sigma_1 \\ \sigma_2 \\ \sigma_4 \\ \sigma_5 \\ \sigma_6 \end{Bmatrix}^{(k)} = \begin{bmatrix} Q_{11} & Q_{12} & 0 & 0 & 0 \\ Q_{12} & Q_{22} & 0 & 0 & 0 \\ 0 & 0 & Q_{44} & 0 & 0 \\ 0 & 0 & 0 & Q_{55} & 0 \\ 0 & 0 & 0 & 0 & Q_{66} \end{bmatrix}^{(k)} \begin{Bmatrix} \varepsilon_1 \\ \varepsilon_2 \\ \varepsilon_4 \\ \varepsilon_5 \\ \varepsilon_6 \end{Bmatrix} \quad (12)$$

In the above equations, the reduced material stiffness coefficients Q_{ij} 's ($i, j = 1, 2, 4, 5, 6$) becomes

$$\begin{aligned} Q_{11}^{(k)} &= Q_{22}^{(k)} = \frac{E^{(k)}}{1 - \nu^{(k)2}}, & Q_{12}^{(k)} &= \frac{\nu^{(k)}E^{(k)}}{1 - \nu^{(k)2}} \\ Q_{66}^{(k)} &= \frac{E^{(k)}}{2(1 + \nu^{(k)})}, & Q_{44}^{(k)} &= Q_{55}^{(k)} = \kappa Q_{66}^{(k)} \end{aligned} \quad (13)$$

where κ is the shear correction factor of FSDT which generally depends on the geometry, material properties and loading conditions. The approximate quantity of $\kappa = 5/6$ or $\kappa = \pi^2/12$ are widely used (Bao and Wang 2019). In this work, the shear correction factor is selected $\kappa = 5/6$.

By measuring the stresses through the conical panel thickness by integration along its direction, the related stress resultants can be achieved as follows:

$$\begin{aligned} (N_{11}, N_{22}, N_{12}) &= \sum_{k=1}^{N_L} \int_{z_k}^{z_{k+1}} (\sigma_1, \sigma_2, \sigma_6)^{(k)} dz \\ (M_{11}, M_{22}, M_{12}) &= \sum_{k=1}^{N_L} \int_{z_k}^{z_{k+1}} z(\sigma_1, \sigma_2, \sigma_6)^{(k)} dz \\ (Q_1, Q_2) &= \sum_{k=1}^{N_L} \int_{z_k}^{z_{k+1}} (\sigma_5, \sigma_4)^{(k)} dz \end{aligned} \quad (14)$$

In the above equations N_{11} , N_{22} , and N_{12} are the membrane stress resultants, M_{11} , M_{22} , and M_{12} are the bending stress resultants and Q_1 and Q_2 indicate the membrane out-of-plane shear stress resultants. The shear membrane stress resultants $N_{12} = N_{21}$ and bending stress resultants $M_{12} = M_{21}$ are considered equal because of elimination of the contribution of $\frac{z}{r(x)}$ in kinematic equations.

Hamilton's principle is also employed to derive the motion equations of the functionally graded GPLRC conical panel. According to this rule, the motion equations of shell on the elastic foundation are derived when the following equation holds (Reddy 2006, Shi et al. 2015)

$$\int_{t_1}^{t_2} (\delta T - \delta V - \delta U) dt = 0 \quad (15)$$

where δT , δU , and δV show the first variation of the kinematic, strain and potential energy of the applied external loads, respectively. The strain energy δU for the composite media in the assumed shell domain can be written as

$$\delta U = \int_0^{\theta_0} \int_{\frac{R_0}{\sin(\beta)}}^{L+\frac{R_0}{\sin(\beta)}} \int_{-0.5h}^{+0.5h} \sigma_i \delta \varepsilon_i r(x) dz dx d\theta, \quad (16)$$

$$i = 1, 2, 4, 5, 6$$

Potential energy δV due to the Winkler-Pasternak elastic foundation for the conical shell are computed as

$$\delta V = \int_0^{\theta_0} \int_{\frac{R_0}{\sin(\beta)}}^{L+R_0/\sin(\beta)} \left[k_w u_3^0 \delta u_3^0 + k_g u_{3,x}^0 \delta u_{3,x}^0 + \frac{k_g}{r(x)^2} u_{3,\theta}^0 \delta u_{3,\theta}^0 \right] r(x) dx d\theta \quad (17)$$

where k_w and k_g are Winkler and Pasternak coefficients of elastic foundation. Also, kinetic energy is determined by the following equation

$$\delta T = \int_0^{\theta_0} \int_{\frac{R_0}{\sin(\beta)}}^{L+R_0/\sin(\beta)} \int_{-0.5h}^{+0.5h} \rho (\dot{u}_1 \delta \dot{u}_1 + \dot{u}_2 \delta \dot{u}_2 + \dot{u}_3 \delta \dot{u}_3) r(x) dz dx d\theta \quad (18)$$

where ρ is the mass density calculated from Eq. (7) for each ply. Also, derivative with respect to time is demonstrated by a ($\dot{\quad}$). Substituting the stress tensor components from Eq. (12) into (16) and employing the variational technique, the motion equations of the functionally graded graphene platelets reinforced composite conical panel resting on two-parameter elastic foundation in terms of the stress resultants are

$$\begin{aligned} \delta u_1^0 &: \frac{1}{r(x)} \{ \sin(\beta) (N_{11} - N_{22}) + r(x) N_{11,x} + N_{12,\theta} \} = I_1 \ddot{u}_1^0 \\ \delta u_2^0 &: \frac{1}{r(x)} \{ 2 \sin(\beta) N_{12} + r(x) N_{12,x} + N_{22,\theta} + \cos(\beta) Q_2 \} = I_1 \ddot{u}_2^0 \\ \delta u_3^0 &: \frac{1}{r(x)} \{ \sin(\beta) Q_1 + r(x) Q_{1,x} + Q_{2,\theta} - \cos(\beta) N_{22} - r(x) k_w u_3^0 + k_g \sin(\beta) u_{3,x}^0 + r(x) k_g u_{3,xx}^0 + \frac{k_g}{r(x)} u_{3,\theta\theta}^0 \} = I_1 \ddot{u}_3^0 \\ \delta \psi_1 &: \frac{1}{r(x)} \{ \sin(\beta) (M_{11} - M_{22}) + r(x) M_{11,x} + M_{12,\theta} - r(x) Q_1 \} = I_3 \ddot{\psi}_1 \\ \delta \psi_2 &: \frac{1}{r(x)} \{ 2 \sin(\beta) M_{12} + r(x) M_{12,x} + M_{22,\theta} - r(x) Q_2 \} = I_3 \ddot{\psi}_2 \end{aligned} \quad (19)$$

The obtained equations of motion in terms of the displacement components for the FG-GPLRC structure may be obtained through Eqs. (14) and (19). The resulting equations are

$$\begin{aligned} A_{11} & \left(u_{1,xx}^0 + \frac{\sin(\beta)}{r(x)} u_{1,x}^0 - \frac{\sin^2(\beta)}{r^2(x)} u_1^0 - \frac{\sin(\beta)}{r^2(x)} u_{2,\theta}^0 - \frac{\sin(\beta) \cos(\beta)}{r^2(x)} u_3^0 \right) \\ & + A_{12} \left(\frac{1}{r(x)} u_{2,x\theta}^0 + \frac{\cos(\beta)}{r(x)} u_{3,x}^0 \right) \\ & + A_{66} \left(\frac{1}{r^2(x)} u_{1,\theta\theta}^0 + \frac{1}{r(x)} u_{2,x\theta}^0 - \frac{\sin(\beta)}{r^2(x)} u_{2,\theta}^0 \right) = I_1 \ddot{u}_1^0 \end{aligned} \quad (20)$$

$$\begin{aligned} A_{11} & \left(\frac{\sin(\beta)}{r^2(x)} u_{1,\theta}^0 + \frac{1}{r^2(x)} u_{2,\theta\theta}^0 + \frac{\cos(\beta)}{r^2(x)} u_{3,\theta}^0 \right) \\ & + \frac{A_{12}}{r(x)} u_{1,x\theta}^0 \\ & + A_{66} \left(\frac{1}{r(x)} u_{1,x\theta}^0 + \frac{\sin(\beta)}{r^2(x)} u_{1,\theta}^0 + u_{2,xx}^0 + \frac{\sin(\beta)}{r(x)} u_{2,x}^0 - \frac{\sin^2(\beta)}{r^2(x)} u_2^0 \right) \\ & + A_{55} \left(\frac{\cos(\beta)}{r^2(x)} u_{3,\theta}^0 - \frac{\cos^2(\beta)}{r^2(x)} u_2^0 + \frac{\cos(\beta)}{r(x)} \psi_2 \right) = I_1 \ddot{u}_2^0 \end{aligned} \quad (21)$$

$$\begin{aligned} A_{55} & \left(u_{3,xx}^0 + \frac{1}{r^2(x)} u_{3,\theta\theta}^0 + \frac{\sin(\beta)}{r(x)} u_{3,x}^0 + \psi_{1,x} + \frac{\sin(\beta)}{r(x)} \psi_1 + \frac{1}{r(x)} \psi_{2,\theta} - \frac{\cos(\beta)}{r^2(x)} u_{2,\theta}^0 \right) \\ & - \frac{A_{11} \cos(\beta)}{r(x)} \left(\frac{1}{r(x)} u_{2,\theta}^0 + \frac{\sin(\beta)}{r(x)} u_1^0 + \frac{\cos(\beta)}{r(x)} u_3^0 \right) \\ & - \frac{A_{12} \cos(\beta)}{r(x)} u_{1,x}^0 - k_w u_3^0 + k_g \left(u_{3,xx}^0 + \frac{\sin(\beta)}{r(x)} u_{3,x}^0 + \frac{1}{r^2(x)} u_{3,\theta\theta}^0 \right) = I_1 \ddot{u}_3^0 \end{aligned} \quad (22)$$

$$\begin{aligned}
D_{11} & \left(\psi_{1,xx} + \frac{\sin(\beta)}{r(x)} \psi_{1,x} - \frac{\sin^2(\beta)}{r^2(x)} \psi_1 - \frac{\sin(\beta)}{r^2(x)} \psi_{2,\theta} \right) \\
& + D_{12} \left(\frac{1}{r(x)} \psi_{2,x\theta} \right) \\
& + D_{66} \left(\frac{1}{r^2(x)} \psi_{1,\theta\theta} + \frac{1}{r(x)} \psi_{2,x\theta} \right. \\
& \left. - \frac{\sin(\beta)}{r^2(x)} \psi_{2,\theta} \right) - A_{55} (u_{3,x}^0 + \psi_1) \\
& = I_3 \ddot{\psi}_1
\end{aligned} \quad (23)$$

$$\begin{aligned}
D_{11} & \left(\frac{\sin(\beta)}{r^2(x)} \psi_{1,\theta} + \frac{1}{r^2(x)} \psi_{2,\theta\theta} \right) + \frac{D_{12}}{r(x)} \psi_{1,x\theta} \\
& + D_{66} \left(\frac{1}{r(x)} \psi_{1,x\theta} + \frac{\sin(\beta)}{r^2(x)} \psi_{1,\theta} \right. \\
& \left. + \psi_{2,xx} + \frac{\sin(\beta)}{r(x)} \psi_{2,x} - \frac{\sin^2(\beta)}{r^2(x)} \psi_2 \right) \\
& - A_{55} \left(\frac{1}{r(x)} u_{3,\theta}^0 - \frac{\cos(\beta)}{r(x)} u_2^0 + \psi_2 \right) \\
& = I_3 \ddot{\psi}_2
\end{aligned} \quad (24)$$

I_1 and I_3 are the inertia terms defined by

$$(I_1, I_3) = \sum_{k=1}^{N_L} \int_{z_k}^{z_{k+1}} \rho^{(k)}(1, z^2) dz \quad (25)$$

Also, In the motion equations, the stretching stiffness coefficients A_{ij} and the bending stiffness coefficients D_{ij} in the composite media are defined as follows

$$(A_{ij}, D_{ij}) = \sum_{k=1}^{N_L} \int_{z_k}^{z_{k+1}} (Q_{ij}^{(k)}, z^2 Q_{ij}^{(k)}) dz, \quad i, j = 1, 2, 4, 5, 6 \quad (26)$$

The equations of motion are accompanied by the boundary conditions. In the following, three kinds of appropriate boundary conditions which are widely used in the open literature are considered, namely the clamped edge boundary conditions (C), the simply supported edge boundary conditions (S) and the free edge boundary conditions (F). Equations describing the boundary conditions on the circumferential edges ($x = \frac{R_0}{\sin(\beta)}$ and

$x = \frac{R_0}{\sin(\beta)} + L$) can be written as follows

$$\text{for simply supported edges (S): } u_1^0 = u_2^0 = u_3^0 = M_{11} = \psi_2 = 0$$

$$\text{for clamped edges (C): } u_1^0 = u_2^0 = u_3^0 = \psi_1 = \psi_2 = 0 \quad (27)$$

$$\text{for free edges (F): } N_{11} = N_{12} = Q_1 = M_{11} = M_{12} = 0,$$

Furthermore, equations describing the boundary conditions on the meridional edges ($\theta = 0$ and $\theta = \theta_0$) can be assumed

$$\text{for simply supported edges (S): } u_1^0 = u_2^0 = u_3^0 = \psi_1 = M_{22} = 0$$

$$\text{for clamped edges (C): } u_1^0 = u_2^0 = u_3^0 = \psi_1 = \psi_2 = 0 \quad (28)$$

$$\text{for free edges (F): } N_{12} = N_{22} = Q_2 = M_{12} = M_{22} = 0,$$

4. GDQ method

There are many nodal point method to discrete the solution domain such as differential quadrature (DQ) method which needs to obtain weighted coefficients for every solution domain. (Shen 2009). Another discretization method that are more stronger but difficult to implement is discrete singular convolution (DSC) method (Civalek 2008, Civalek and Acar 2007, Civalek 2009, Akgöz and Civalek 2011). The GDQ method is an approximate but efficient numerical tool for discretization the first, second and higher order derivatives of each point in the panel domain. Applying this method to governing equations is simpler rather than other techniques. This method relies on converting any unknown function \mathbf{u} derivative at any point into a linear sum of weighting coefficients and function values at some defined distributed points in the domain. For instance applying the GDQ approach to the first and second order derivatives given as follow (Tornabene *et al.* 2009, Javani *et al.* 2019)

$$\begin{aligned}
\mathbf{u}_{,x} |_{x=x_p, \theta=\theta_q} &= \sum_{p'=1}^{N_x} \sum_{q'=1}^{N_\theta} C_{pp'}^x \delta_{qq'}^\theta \mathbf{u} |_{x=x_{p'}, \theta=\theta_{q'}} \\
\mathbf{u}_{,\theta} |_{x=x_p, \theta=\theta_q} &= \sum_{p'=1}^{N_x} \sum_{q'=1}^{N_\theta} \delta_{pp'}^x C_{qq'}^\theta \mathbf{u} |_{x=x_{p'}, \theta=\theta_{q'}} \\
\mathbf{u}_{,x\theta} |_{x=x_p, \theta=\theta_q} &= \sum_{p'=1}^{N_x} \sum_{q'=1}^{N_\theta} C_{pp'}^x C_{qq'}^\theta \mathbf{u} |_{x=x_{p'}, \theta=\theta_{q'}} \\
\mathbf{u}_{,xx} |_{x=x_p, \theta=\theta_q} &= \sum_{p'=1}^{N_x} \sum_{q'=1}^{N_\theta} \bar{C}_{pp'}^x \delta_{qq'}^\theta \mathbf{u} |_{x=x_{p'}, \theta=\theta_{q'}} \\
\mathbf{u}_{,\theta\theta} |_{x=x_p, \theta=\theta_q} &= \sum_{p'=1}^{N_x} \sum_{q'=1}^{N_\theta} \delta_{pp'}^x \bar{C}_{qq'}^\theta \mathbf{u} |_{x=x_{p'}, \theta=\theta_{q'}}, \quad p = 1, 2, \dots, N_x, \quad q = 1, 2, \dots, N_\theta
\end{aligned} \quad (29)$$

in which N_φ and N_θ are the number of grid points in the φ and θ -directions, respectively. $\delta_{pp'}^\varphi$ and $\delta_{qq'}^\theta$ are set to one when $p = p'$ and $q = q'$. Also, $C_{pp'}^\varphi$ and $C_{qq'}^\theta$

indicate the weighting coefficients of the first order and $\bar{C}_{pp'}^\varphi$ and $\bar{C}_{qq'}^\theta$ denote the weighting coefficients of the second order derivatives, respectively. Using the Lagrange interpolated polynomials, and its derivatives the weighting coefficients can be calculated

$$C_{pp'}^x = \begin{cases} \frac{\Pi(x_p)}{(x_p - x_{p'})\Pi(x_{p'})} & \text{when } p \neq p' \\ -\sum_{k=1, k \neq p}^{N_x} C_{pk}^x & \text{when } p = p' \end{cases} \quad (30)$$

$$C_{qq'}^\theta = \begin{cases} \frac{\Pi(\theta_q)}{(\theta_q - \theta_{q'})\Pi(\theta_{q'})} & \text{when } q \neq q' \\ -\sum_{k=1, k \neq q}^{N_\theta} C_{qk}^\theta & \text{when } q = q' \end{cases}$$

$p, p' = 1, 2, \dots, N_x \quad q, q' = 1, 2, \dots, N_\theta$

in which

$$\Pi(x_p) = \prod_{k=1, k \neq p}^{N_x} (x_p - x_k), \quad (31)$$

$$\Pi(\theta_q) = \prod_{k=1, k \neq q}^{N_\theta} (\theta_q - \theta_k)$$

and

$$\left(\bar{C}_{pp'}^x = 2 \left(C_{pp}^x C_{pp'}^x - \frac{C_{pp'}^x}{(x_p - x_{p'})} \right), \quad p \neq p' \right.$$

$$\left. p, p' = 1, 2, \dots, N_x \right.$$

$$\left(\bar{C}_{pp}^x = -\sum_{k=1, k \neq p}^{N_x} \bar{C}_{pk}^x, \quad p = p', \right.$$

$$\left. p = 1, 2, \dots, N_x \right. \quad (32)$$

$$\left(\bar{C}_{qq'}^\theta = 2 \left(C_{qq}^\theta C_{qq'}^\theta - \frac{C_{qq'}^\theta}{(\theta_q - \theta_{q'})} \right), \quad q \neq q' \right.$$

$$\left. q, q' = 1, 2, \dots, N_\theta \right.$$

$$\left(\bar{C}_{qq}^\theta = -\sum_{k=1, k \neq q}^{N_\theta} \bar{C}_{qk}^\theta, \quad q = q' \right.$$

$$\left. q = 1, 2, \dots, N_\theta \right.$$

Type of the grid point distribution plays a significant role in the accuracy of this method. The conical panel domain must be discrete base on a specific grid dispensation. In the current research, the Gauss-Chebyshev-Lobatto grid distribution is applied owing its stability and accuracy. In this type dispensation, the discrete points in the x and θ -directions are written as

$$x_p = L \left(\frac{1}{2} - \frac{1}{2} \cos \left(\frac{p-1}{N_x-1} \pi \right) \right) + \frac{R_0}{\sin(\beta)}, \quad (33)$$

$p = 1, 2, \dots, N_x$

$$\theta_q = \theta_0 \left(\frac{1}{2} - \frac{1}{2} \cos \left(\frac{q-1}{N_\theta-1} \pi \right) \right), \quad (34)$$

$q = 1, 2, \dots, N_\theta$

The discretized equations of motion and associated boundary conditions after implementing the GDQ method are not given here for the sake of brevity; meanwhile, one may refer to the other available works, e.g. (Tornabene *et al.* 2009, Javani *et al.* 2020). In the following formula the matrix form of derived algebraic eigenvalue is demonstrated

$$\mathbf{M}\{\ddot{u}\} + \mathbf{K}\{u\} = 0 \quad (35)$$

where $\{u\}$ is the displacement vector which has $(5 \times N_x \times N_\theta)$ components and includes unknown displacements constituents $(u_{1pq}^0, u_{2pq}^0, u_{3pp}^0, \psi_{1pq}, \psi_{2pq})$. Moreover, $[\mathbf{M}]$ denotes the mass matrix and $[\mathbf{K}]$ is the stiffness matrix. Since the free vibration analysis of the FG-GPLRC conical panel on the two parameter elastic foundation is a harmonic motion, one may suppose the following periodic relation for the displacement functions

$$u_1^0(x, \theta, t) = U_1^0(x, \theta) \sin(\omega t + \alpha)$$

$$u_2^0(x, \theta, t) = U_2^0(x, \theta) \sin(\omega t + \alpha)$$

$$u_3^0(x, \theta, t) = U_3^0(x, \theta) \sin(\omega t + \alpha) \quad (36)$$

$$\psi_1(x, \theta, t) = \Psi_1(x, \theta) \sin(\omega t + \alpha)$$

$$\psi_2(x, \theta, t) = \Psi_2(x, \theta) \sin(\omega t + \alpha)$$

Applying Eq. (36) into (35), the matrix form of algebraic eigenvalue equations for the natural frequencies and the corresponding mode shapes of the conical panel can be obtained

$$(\mathbf{K} - \omega^2 \mathbf{M})\mathbf{U} = 0 \quad (37)$$

where ω and \mathbf{U} are the natural frequency and the corresponding mode shape.

5. Results and discussion

The extended procedure in the previous section is exerted here to study the free vibration characteristics of FG-GPLRC conical panel resting on Winkler-Pasternak elastic foundation. Unless otherwise mentioned, the nanocomposite is constructed by mixing the isotropic epoxy matrix and graphene platelets. The mechanical properties for these constituents are listed in Table 1.

Table 1 mechanical properties of the matrix and GPLs. (Wu *et al.* 2017)

Properties	Epoxy	GPL
Elasticity modulus(E)[GPa]	3.0	1010
Mass density (ρ) [kg/m ³]	1200	1062.5
Poisson's ratio (ν)	0.34	0.186

Table 2 Convergence test of the first three dimensionless frequency for X-GPLRC conical panel with different boundary conditions

B.Cs.	mode	$N_x=N_\theta$	N_L						
			4	6	8	10	12	20	40
FSFS	Ω_1	15	0.6630	0.6687	0.6706	0.6715	0.6720	0.6727	0.6730
		17	0.6625	0.6682	0.6702	0.6711	0.6716	0.6723	0.6726
		19	0.6623	0.6680	0.6700	0.6709	0.6714	0.6721	0.6724
		21	0.6622	0.6679	0.6698	0.6707	0.6712	0.6720	0.6723
	Ω_2	15	0.7689	0.7782	0.7813	0.7828	0.7836	0.7848	0.7852
		17	0.7691	0.7784	0.7816	0.7830	0.7838	0.7850	0.7855
		19	0.7692	0.7785	0.7817	0.7832	0.7839	0.7851	0.7856
		21	0.7693	0.7786	0.7817	0.7832	0.7840	0.7852	0.7856
	Ω_3	15	1.3301	1.3352	1.3369	1.3378	1.3382	1.3389	1.3391
		17	1.3302	1.3353	1.3371	1.3379	1.3383	1.3390	1.3393
		19	1.3303	1.3353	1.3371	1.3379	1.3384	1.3390	1.3393
		21	1.3303	1.3354	1.3371	1.3380	1.3384	1.3391	1.3393
CCCC	Ω_1	15	1.9076	1.9280	1.9350	1.9383	1.9400	1.9426	1.9437
		17	1.9076	1.9280	1.9350	1.9383	1.9401	1.9426	1.9437
		19	1.9076	1.9280	1.9350	1.9383	1.9401	1.9426	1.9437
		21	1.9076	1.9280	1.9350	1.9383	1.9401	1.9426	1.9437
	Ω_2	15	2.0228	2.0358	2.0403	2.0423	2.0434	2.0450	2.0457
		17	2.0228	2.0358	2.0403	2.0423	2.0434	2.0450	2.0457
		19	2.0228	2.0358	2.0403	2.0423	2.0434	2.0450	2.0457
		21	2.0228	2.0358	2.0403	2.0423	2.0434	2.0450	2.0457
	Ω_3	15	2.6849	2.7163	2.7271	2.7321	2.7349	2.7388	2.7405
		17	2.6849	2.7163	2.7271	2.7321	2.7349	2.7388	2.7405
		19	2.6849	2.7163	2.7271	2.7321	2.7349	2.7388	2.7405
		21	2.6849	2.7163	2.7271	2.7321	2.7349	2.7388	2.7405

Several types of boundary conditions with the combination of clamped (C), simply-supported (S), and free (F) are utilized at the meridional and circumferential edges of conical panels. For example, the FCSF boundary condition illustrate a panel is free at $\theta = 0$, clamped at $x = \frac{R_0}{\sin(\beta)} + L$, simply-support at $\theta = \theta_0$ and eventually, free at $x = \frac{R_0}{\sin(\beta)}$.

In the present manuscript, to study the influences of elastic coefficients on natural frequencies of the panel, the nondimensional Winkler and Pasternak coefficients are setup according to as

$$K_w = \frac{k_w R_0^4 (1 - \nu_m^2)}{E_m h^3} \quad (38)$$

$$K_g = \frac{k_g R_0^2 (1 - \nu_m^2)}{E_m h^3}$$

Also, the nondimensional natural frequencies of the introduced structure are defined as

$$\Omega_i = \omega_i R_0^2 \sqrt{\frac{\rho_m (1 - \nu_m^2)}{E_m h^2}} \quad (39)$$

Length of graphene platelets is set $a_{GPL} = 2.5\mu\text{m}$, its width $b_{GPL} = 1.5\mu\text{m}$ and finally, its thickness is assumed $t_{GPL} = 1.5\text{nm}$ in all of the numerical results.

5.1 Convergence and Comparison Study

A convergence analysis is provided on the free vibration characteristics to optimize the number of layers and the required number of grid points to reach the converged natural frequencies. In the current example, the number of grid points in the meridional direction and in the circumferential direction are the same $N_x = N_\theta$.

Table 2 gives the converged first three dimensionless natural frequencies of a FG-GPLRC conical panel with geometrical parameters of $\frac{h}{R_0} = 0.2$, $\frac{L}{R_0} = 4$, $\beta = 45^\circ$ and $\theta_0 = 120^\circ$. For developing the numerical results of this Table, the weight fraction of GPLs is assumed $W_{GPL} = 0.5\%$, moreover X-type functionally graded pattern is selected. In this study, two types of boundary conditions FSFS and CCCC are assumed to model the shell. As it can be seen, the results converged for 21 grid points in each direction specially for CCCC panel. Another result of this study is a small difference between the natural frequencies

Table 3 Comparison of the frequency parameters $\Omega = \omega R \sqrt{\rho(1 - \nu^2)/E}$ for an isotropic FS hemispherical shell ($\varphi_{in} = 0$, $\varphi_{out} = 90^\circ$ and $R = 1\text{m}$)

modes	conical			cylindrical			annular		
	FCFC	SFSF	FSSF	FCFC	SFSF	FSSF	FCFC	SFSF	FSSF
Present	122.742	74.271	90.919	204.906	168.111	76.197	235.467	13.519	57.677
Tornabene <i>et al.</i> (2009)	122.73	74.28	90.92	204.87	168.18	76.18	235.47	13.52	57.68
Present	135.298	125.316	170.080	223.034	364.305	188.044	249.301	76.326	150.273
Tornabene <i>et al.</i> (2009)	135.28	125.33	170.04	222.97	364.40	188.14	249.30	76.326	150.27
Present	241.427	224.779	232.290	383.357	407.053	232.304	307.526	159.111	233.133
Tornabene <i>et al.</i> (2009)	241.48	224.79	232.33	383.58	407.33	232.26	307.53	159.11	233.13
Present	256.546	258.795	272.365	440.777	421.556	285.348	424.246	167.867	288.568
Tornabene <i>et al.</i> (2009)	256.59	258.79	272.43	441.11	421.67	285.37	424.25	167.87	288.57
Present	287.244	288.676	312.849	468.076	634.226	428.674	592.675	287.650	401.527
Tornabene <i>et al.</i> (2009)	287.24	288.70	312.85	467.98	634.29	428.84	592.67	287.65	401.53
Present	293.441	327.003	324.563	474.874	651.573	467.638	628.392	315.231	456.916
Tornabene <i>et al.</i> (2009)	293.42	327.04	324.61	474.78	651.69	467.63	628.39	315.23	456.92
Present	381.132	360.895	374.648	714.702	717.979	537.115	648.642	399.784	588.038
Tornabene <i>et al.</i> (2009)	381.19	360.93	374.71	715.01	717.89	537.52	648.64	399.78	588.04
Present	421.566	388.159	411.080	718.619	780.625	573.671	729.722	434.010	619.547
Tornabene <i>et al.</i> (2009)	421.65	388.22	411.13	719.14	781.15	573.73	729.72	434.01	619.55
Present	463.562	444.377	454.818	724.986	792.691	673.315	795.338	505.973	650.908
Tornabene <i>et al.</i> (2009)	463.67	444.46	454.88	725.44	792.79	673.55	795.34	505.97	650.91
Present	494.978	480.373	488.313	737.303	806.677	731.644	876.766	604.968	763.197
Tornabene <i>et al.</i> (2009)	494.98	480.42	488.36	736.76	806.95	731.76	876.77	604.97	763.19

at $N_L = 10$ and $N_L > 10$; Hence a laminated GPLRC panel consists 10 layers could offer adequate accuracy to design an appropriate functionally graded panel with smooth changes between material compositions and properties. In the parametric studies the number of layers is selected $N_L = 10$.

To validate the formulations and employed method, the free vibration of conical, cylindrical panels and sector plates may be considered. Table 3 compares the results of this study for a pure isotropic panel and plate, where $E = 2.1 \times 10^{11}\text{Pa}$, $\rho = 7800\text{kg/m}^3$ and $\nu = 0.3$, with those addressed in (Tornabene *et al.* 2009). Table 3 indicates the first ten natural frequencies $f(\text{Hz})$ versus the boundary conditions (FCFC, SFSF, FSSF). The geometrical parameters of each structure are given as follow

- Conical panel: $R_0 = 0.5\text{ m}$, $h = 0.1\text{ m}$, $L = 2/\cos(\beta)\text{m}$, $\beta = 40^\circ$, $\theta_0 = 120^\circ$
- Cylindrical panel: $R_0 = 1\text{ m}$, $h = 0.1\text{ m}$, $L = 2\text{ m}$, $\beta = 0^\circ$, $\theta_0 = 120^\circ$
- Sector plate: $R_0 = 0.5\text{ m}$, $h = 0.1\text{ m}$, $L = 1.5\text{ m}$, $\beta = 90^\circ$, $\theta_0 = 120^\circ$

Close agreement is observed between the obtained results and those reported based on the GDQ method by Tornabene *et al.* (2009).

A second comparison analysis is performed in Table 4 between calculated results of this manuscript and those reported based on the experimental and theoretical study by Bardell *et al.* (1998) and Ritz method by Kiani *et al.* (2018). The mechanical properties of the isotropic homogeneous

Aluminium conical panel are $E = 70\text{GPa}$, $\rho = 2700\text{kg/m}^3$ and $\nu = 0.3$. The comparison is examined for two panels; The first panel is introduced with $R_0 = 16\text{cm}$, $h = 2\text{mm}$, $L = 112\text{cm}$, $\beta = 26.5^\circ$ and $\theta_0 = 180^\circ$ while the other one had following parameters $R_0 = 34\text{cm}$, $h = 2\text{mm}$, $L = 114\text{cm}$, $\beta = 3.8^\circ$ and $\theta_0 = 130^\circ$. It can be seen that the determined first ten natural frequencies $f(\text{Hz})$ in the present paper are well compared with the literature.

As mentioned in the introduction section, no paper has yet reported the free vibration of FG-GPLRC conical panels. Therefore, to carry out a comparison evaluation, the present problem is restricted to the case of a closed FG-GPLRC annular plate. The conical panel can be reduce to the annular plate considering $\beta = 90^\circ$ and applying kinematical and physical compatibility conditions for the straight edges. This structure is analyzed by Malekzadeh *et al.* (2018) by means of the transformed differential quadrature method. For the sake of comparison, a conical panel with $R_0 = 0.25\text{m}$, $h = 0.1\text{m}$, $L = 0.75\text{m}$ and $\theta_0 = 360^\circ$ is considered. The results are compared in terms of fundamental frequency parameter $\lambda = \omega h \sqrt{\rho_m/E_m}$ for four functionally graded patterns and three types of boundary conditions (CC, CS, CF) at the inner and outer circumferential edges, respectively, in Table 5. It is concluded that good agreement between the results of this study and those obtained by Malekzadeh *et al.* (2018) which guarantees the accuracy and efficiency of the proposed formulations and method.

Table 4 Comparison of the first ten frequencies f(Hz) for isotropic conical panel with FFFF boundary condition

Present	Bardell <i>et al.</i> (1998) (Exp.)	Bardell <i>et al.</i> (1998)	Kiani <i>et al.</i> (2018)	Present	Bardell <i>et al.</i> (1998) (Exp.)	Bardell <i>et al.</i> (1998)	Kiani <i>et al.</i> (2018)
4.437	4.5	4.65	4.274	6.697	7.5	7.21	6.568
8.437	8.9	8.75	8.203	12.628	12.7	12.32	12.595
11.357	11.5	11.32	11.123	19.048	18.2	18.21	18.807
20.911	20.9	20.85	20.695	35.314	35.6	34.40	35.246
22.286	21.7	22.63	21.724	45.767	46.0	44.32	45.579
32.841	33.2	33.06	32.888	69.252	59.5	67.78	68.829
46.751	46.6	47.83	47.434	75.825	70.4	75.43	75.963
47.482	47.4	47.87	48.309	76.041	43.1	76.05	77.311
62.984	58.6	63.51	66.261	90.181	90.4	87.80	88.522
67.228	63.7	67.95	68.261	116.288	-	113.65	116.545

Table 5 Comparison of natural frequency parameter $\lambda = \omega h \sqrt{\rho_m/E_m}$ for a FG-GPLRC annular plate with weight fraction of reinforcements $W_{GPL} = 1\%$

Graded type	Source	B.Cs.		
		CC	CS	CF
U-GPLRC	Present	0.2207	0.1526	0.0344
	Malekzadeh <i>et al.</i> (2018)	0.22095	0.15274	0.03445
X-GPLRC	Present	0.2485	0.1740	0.0398
	Malekzadeh <i>et al.</i> (2018)	0.24454	0.17090	0.03899
O-GPLRC	Present	0.1829	0.1246	0.0277
	Malekzadeh <i>et al.</i> (2018)	0.19038	0.13001	0.02898

5.2 Parametric study

After providing the comparison analysis with the open literature, in this section, novel numerical results from the present study are illustrated.

The first five dimensionless natural frequencies of the FG-GPLRC conical panels for three types of functionally graded patterns with various GPL weight fraction are presented in Table 6. The results are obtained for a conical panel with $\frac{h}{R_0} = 0.2, L/R_0 = 4, \beta = 45^\circ$ and $\theta_0 = 120^\circ$. This Table lists the natural frequencies for three different boundary conditions including CCCC, CSCS and CCFE. The results exhibit that for X-GPLRC, the natural frequencies have the highest value. Inversely, the functionally graded O pattern feature the lowest natural frequencies. Moreover, it is demonstrated that an increased GPL enrichment from $W_{GPL} = 0.1\%$ to $W_{GPL} = 1\%$, yields an enhancement in the natural frequency for all the boundary conditions. Finally, it is seen that, the stiffer edges result in the stiffer structure and hence higher frequency parameters.

To investigate the influence of elastic foundation and length-to-radius ratio of X-GPLRC conical panels, a parametric analysis is conducted and the first five nondimensional natural frequencies are illustrated in Table 7. For each values of the Length-to-radius ratio, the frequency parameters are given for three values of the semi-vertex angle. Fully clamped (CCCC) nanocomposite

conical panel with angle of embrace $\theta_0 = 90^\circ$ and thickness-to-radius ratio $h/R_0 = 0.2$ is considered. The weight fraction of graphene platelets is assumed $W_{GPL} = 1\%$. The numerical results reveal the key role of the Winkler-Pasternak coefficients in enhancing the nondimensional natural frequencies. As the numerical results demonstrate, higher L/R_0 and β led to lower nondimensional natural frequencies of clamped conical panel due to the less rigidity.

The subsequent parametric study is examined to analyse the effect of the shell thickness on the fundamental frequency as shown in Table 8. In this example, the fundamental dimensionless frequency is obtained for various angle of embrace and different boundary conditions. Other geometrical parameters are $L/R_0 = 4$ and $\beta = 45^\circ$. To develop this study X-GPLRC conical panel with 1% nanofiller weight fraction on an elastic foundation with nondimensional Winkler-Pasternak $(K_w, K_g) = (200, 20)$ is considered. It is seen that higher thickness-to-radius ratio produce looser frequency parameters. It is worth noting that the increase in the thickness-to-radius ratio makes the more stable structure; hence the natural frequency will be increased, but the non-dimensional frequency decreases. Table 8 shows that the dimensionless frequency of any boundary conditions decrease with increasing the angle of embrace θ_0 except for the FCFC and FSFS.

Fig. 2 indicates the variation of fundamental dimensionless frequency versus semi-vertex angle β for

Table 6 First five dimensionless frequency of FG-GPLRC conical panel respect to various reinforcement weight fraction and FG pattern with different boundary conditions

B.Cs.	W_{GPL}	Graded type	Ω_1	Ω_2	Ω_3	Ω_4	Ω_5	
CCCC	0.1	U	1.267	1.373	1.776	2.061	2.160	
		X	1.310	1.405	1.840	2.114	2.243	
		O	1.221	1.336	1.710	2.004	2.071	
	0.5	U	1.791	1.941	2.510	2.913	3.052	
		X	1.938	2.042	2.732	3.094	3.333	
		O	1.621	1.785	2.278	2.697	2.716	
	1	U	2.283	2.474	3.199	3.713	3.890	
		X	2.511	2.628	3.545	3.994	4.323	
		O	2.011	2.212	2.836	3.343	3.363	
	CSCS	0.1	U	1.145	1.249	1.602	1.865	1.937
			X	1.180	1.276	1.657	1.907	2.010
			O	1.108	1.217	1.547	1.820	1.860
0.5		U	1.618	1.766	2.264	2.636	2.738	
		X	1.740	1.850	2.455	2.778	2.985	
		O	1.481	1.630	2.073	2.448	2.465	
1		U	2.063	2.251	2.886	3.360	3.489	
		X	2.251	2.378	3.183	3.579	3.872	
		O	1.843	2.022	2.588	3.024	3.081	
CCFF		0.1	U	0.434	0.875	1.049	1.252	1.550
			X	0.450	0.906	1.077	1.295	1.597
			O	0.417	0.840	1.018	1.208	1.497
	0.5	U	0.614	1.237	1.482	1.770	2.190	
		X	0.667	1.341	1.576	1.918	2.347	
		O	0.549	1.102	1.362	1.612	1.978	
	1	U	0.783	1.577	1.890	2.256	2.792	
		X	0.864	1.736	2.033	2.488	3.033	
		O	0.677	1.357	1.692	2.006	2.440	

X-GPLRC conical panel with 1% reinforcements weight fraction W_{GPL} and different elastic foundation coefficients (K_w, K_g). This figure is provided for SSSS boundary condition. figure is drawn for three non-dimensional parameters $L/R_0 = 2, 4, 6$. In this subsequent section thickness-to-radius ratio $h/R_0 = 0.1$ and embrace angle $\theta_0 = 90^\circ$ is assumed. The mentioned figure presents that the fundamental frequency of nanocomposite conical panel decreases as the semi-vertex increases from $\beta = 0$ to $\beta = 90^\circ$.

Furthermore, it is observed that the effect of elastic foundation decreases as the semi-vertex angle and length-to-radius ratio increase.

Influences of the angle of embrace on the fundamental dimensionless frequency of X-GPLRC conical panel are drawn in Fig. 3-4. The numerical results are depicted for various thickness-to-radius ratios $h/R_0 = 0.05, 0.1, 0.5$.

Fig. 3 is related to SSSS panel and Fig. 4 represent the case for FSFS panel. Each figure consists four sub-figure that are provided for various semi-vertex angle $\beta =$

$0, 30^\circ, 60^\circ, 90^\circ$. For developing the current example, length-to-radius ratio $L/R_0 = 4$ and nanofiller weight fraction $W_{GPL} = 1\%$ is considered. As seen from these figures, higher embrace angle produces lower frequency parameter and decreases the effect of thickness-to-radius ratio for SSSS conical panel; while it gives rise to higher frequency parameter and increases the effect of thickness-to-radius ratio for FSFS conical panel. Also, the effect of thickness-to-radius ratio is diminished, when semi-vertex angle β increases.

Fig. 5 aims to investigate the influence of reinforcement weight fraction W_{GPL} on the fundamental natural frequency. In this study, GPLRC laminated conical panel is examined with $h/R_0 = 0.05$, $L/R_0 = 4$, $\beta = 45^\circ$, $\theta_0 = 120^\circ$ and $(K_w, K_g) = (100, 10)$, at different functionally types. Four type of boundary conditions are supposed. It can be concluded that for all selected boundary conditions, the natural frequency of the shell increases by augmentation the GPL weight fraction. Also, it is verified that among the various functionally graded patterns, FG-X type results in

Table 7 First five dimensionless frequency of CCCC X-GPLRC conical panel respect to various length-to-radius ratio and semi-vertex angle with different Winkler-Pasternak coefficients

(K_w, K_g)	L/R_0	β	mode				
			Ω_1	Ω_2	Ω_3	Ω_4	Ω_5
(0,0)	2	30	6.872	8.337	11.174	12.889	13.316
		45	5.731	7.299	10.385	10.883	12.388
		60	4.901	6.641	9.684	9.905	11.804
	4	30	3.873	4.123	5.255	6.246	6.587
		45	2.839	3.227	4.234	4.937	5.258
		60	2.101	2.718	3.552	4.104	4.681
	6	30	2.519	2.670	3.521	3.833	4.021
		45	1.868	1.870	2.635	2.832	3.035
		60	1.316	1.504	2.040	2.249	2.585
(200,0)	2	30	14.548	15.487	17.398	17.834	18.165
		45	14.081	15.079	16.555	17.066	17.472
		60	13.818	14.848	15.813	16.861	16.967
	4	30	10.068	10.213	12.093	14.266	14.812
		45	9.054	9.584	11.065	13.699	14.158
		60	8.395	9.349	10.491	12.952	13.755
	6	30	7.320	7.801	9.141	11.517	11.678
		45	6.658	6.803	8.054	10.355	10.579
		60	6.057	6.557	7.495	9.392	9.972
(0,20)	2	30	11.787	14.491	17.639	18.093	19.227
		45	10.741	13.620	16.055	17.312	18.547
		60	10.074	13.213	14.753	17.144	18.064
	4	30	7.175	9.135	9.784	10.678	11.490
		45	6.086	8.096	9.165	9.745	9.904
		60	5.455	7.597	8.707	8.820	9.480
	6	30	5.281	6.719	7.022	7.777	8.488
		45	4.343	5.795	6.371	7.031	7.046
		60	3.821	5.357	6.018	6.230	6.648
(200,20)	2	30	15.640	17.604	18.397	19.837	22.126
		45	14.632	17.235	17.808	18.993	20.642
		60	14.041	17.060	17.428	18.516	19.806
	4	30	10.090	10.367	12.257	15.509	15.717
		45	9.101	9.600	11.109	14.183	14.533
		60	8.409	9.357	10.503	13.055	13.877
	6	30	7.328	7.838	9.182	11.569	11.759
		45	6.668	6.809	8.065	10.382	10.606
		60	6.060	6.560	7.498	9.399	9.982

the highest natural frequency while the O-distribution type results in the lowest natural frequency.

The first six mode shapes of X-GPLRC conical panel with FCFC boundary condition are given in Fig. 6. This study is performed for clarify the vibration response of the mentioned nanocomposite structure without elastic foundation. The nanofillers fraction is $W_{GPL} = 1\%$; Furthermore, the geometrical parameters $h/R_0 = 0.05$, $L/R_0 = 4$, $\beta = 45^\circ$ and $\theta_0 = 120^\circ$ are considered.

In Fig. 7 the effect of elastic foundation on the fundamental frequency and corresponding mode shape of a X-GPLRC conical panel with two types of boundary conditions (FCFC, FFCC) is depicted. The thickness ratio $h/R_0 = 0.05$, the length ratio $L/R_0 = 4$, the semi-vertex angle $\beta = 30^\circ$ and the embrace angle $\theta_0 = 120^\circ$ are considered. As can be observed, the magnitudes of the Winkler-Pasternak coefficients have an important affect the frequencies and corresponding mode shapes.

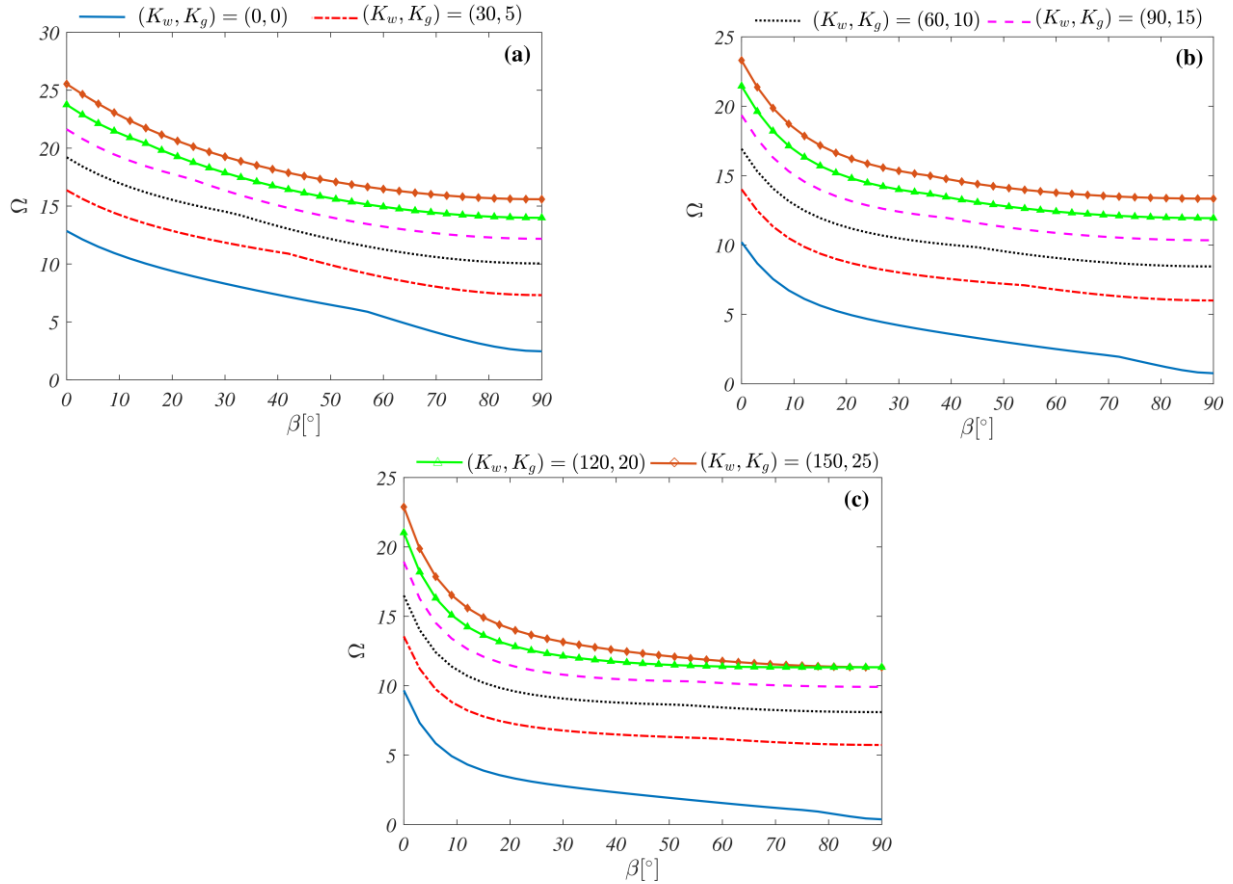


Fig. 2 Fundamental dimensionless frequency of SSSS X-GPLRC conical panel with respect to semi-vertex angle for various elastic foundation coefficients . (a: $L/R_0 = 2$, b: $L/R_0 = 4$, c: $L/R_0 = 6$)

Table 8 Fundamental dimensionless frequency of X-GPLRC conical panel respect to thickness-to-radius ratio and embrace angle with different boundary conditions

		B.Cs.							
(h/R_0)	θ_0	CCCC	CSCS	CFCF	SCSC	SSSS	SFSF	FCFC	FSFS
60	90	16.580	16.467	13.452	16.430	16.328	13.404	8.171	8.171
	120	13.977	13.950	8.251	13.853	13.824	8.204	9.087	9.087
	60	11.158	11.158	6.930	11.153	11.152	6.927	4.087	4.087
0.1	90	15.775	15.714	10.154	15.512	15.457	10.114	8.792	8.791
	120	7.581	7.580	4.257	7.574	7.573	4.252	4.547	4.547
0.2	90	9.101	9.100	5.197	9.089	9.088	5.194	4.399	4.398
	120	4.472	4.472	2.779	4.472	4.472	2.779	1.637	1.636
0.5	90	3.672	3.672	2.090	3.671	3.671	2.089	1.761	1.761
	120	3.059	3.059	1.718	3.058	3.058	1.717	1.820	1.820

6. Conclusions

In the present paper, the free vibration analysis of a functionally graded laminated conical panel reinforced with graphene platelets is examined. The equations of motion are derived using the first order shear deformation theory, the Sanders kinematic assumption and Hamilton's principle. After discretization the motion equations by implementing

the GDQ method, eigenvalue problem is solved. Based on the calculated natural frequencies and obtained corresponding mode shapes:

- Graphene platelets weight fraction and patterns of distribution in the thickness direction are two effective parameters on the free vibration characteristics of FG-GPLRC conical panel. The higher reinforcement weight fraction produce the higher dimensionless natural frequencies. Moreover, a shell with FG-X pattern is associated most natural frequency along types of dispersion.
- Semi-vertex angle β , length-to-radius L/R_0 ratio and thickness-to-radius ratio h/R_0 rise result in decrease non-dimensional natural frequencies of the structure.
- Embrace angle of the panel is an important factor in the free vibration behavior of the conical panel.
- It is found that the boundary conditions of the conical panel plays a key role on the natural frequencies and associated mode shapes.
- higher Winkler-Pasternak coefficients enhance the stability of the FG-GPL nanocomposite shell and so the natural frequency parameters tend to larger value.

Acknowledgments

This research is funded by the Vietnam National Foundation for Science and Technology Development (NAFOSTED) under grant number 107.99-2019.02.

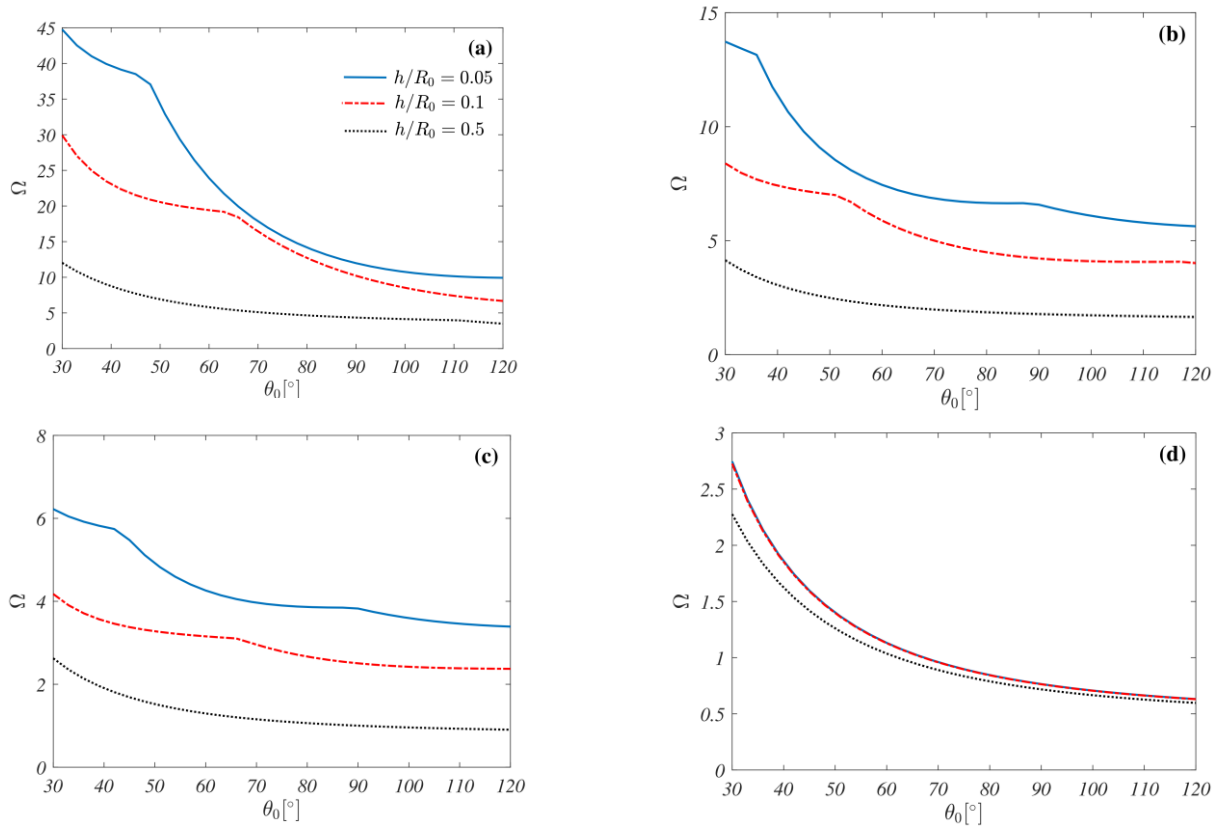


Fig. 3 Fundamental dimensionless frequency of SSSS X-GPLRC conical panel with respect to embrace angle for various thickness-to-radius ratio. (a: $\beta = 0^\circ$, b: $\beta = 30^\circ$, c: $\beta = 60^\circ$, d: $\beta = 90^\circ$)

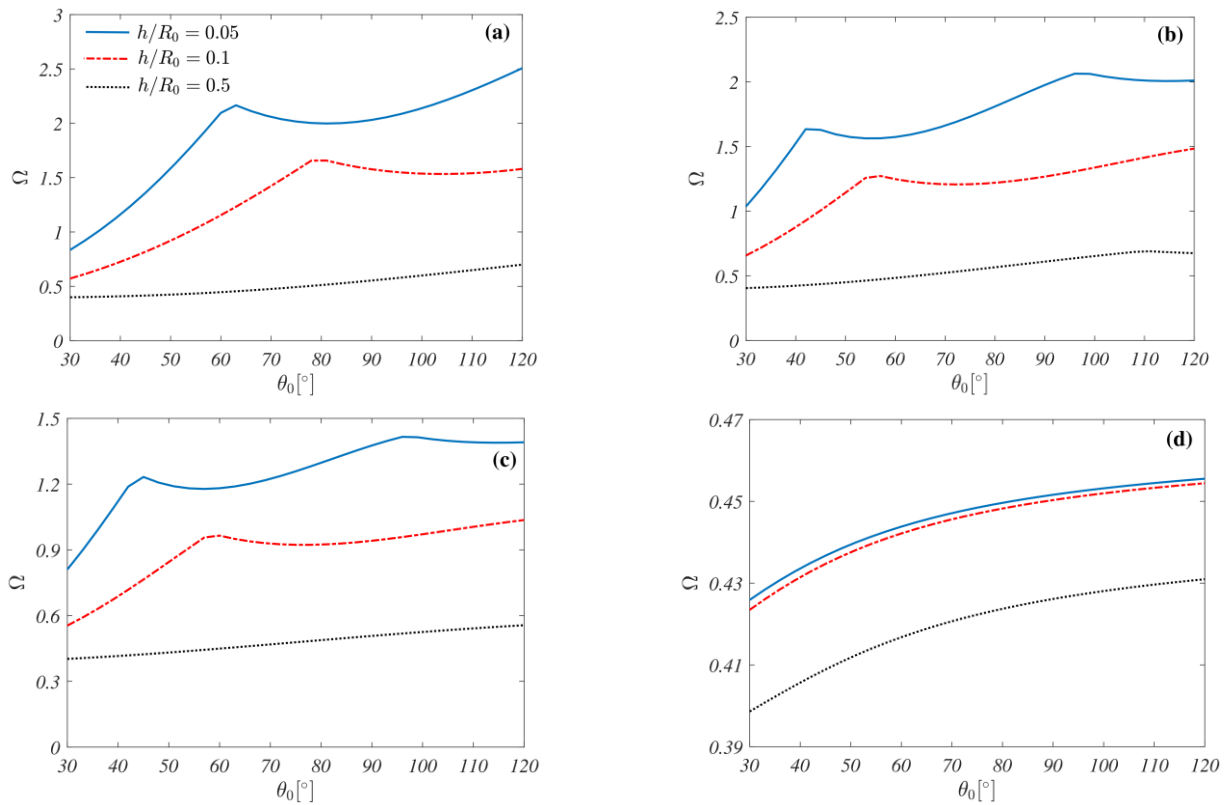


Fig. 4 Fundamental dimensionless frequency of FSFS X-GPLRC conical panel with respect to embrace angle for various thickness-to-radius ratio. (a: $\beta = 0^\circ$, b: $\beta = 30^\circ$, c: $\beta = 60^\circ$, d: $\beta = 90^\circ$)

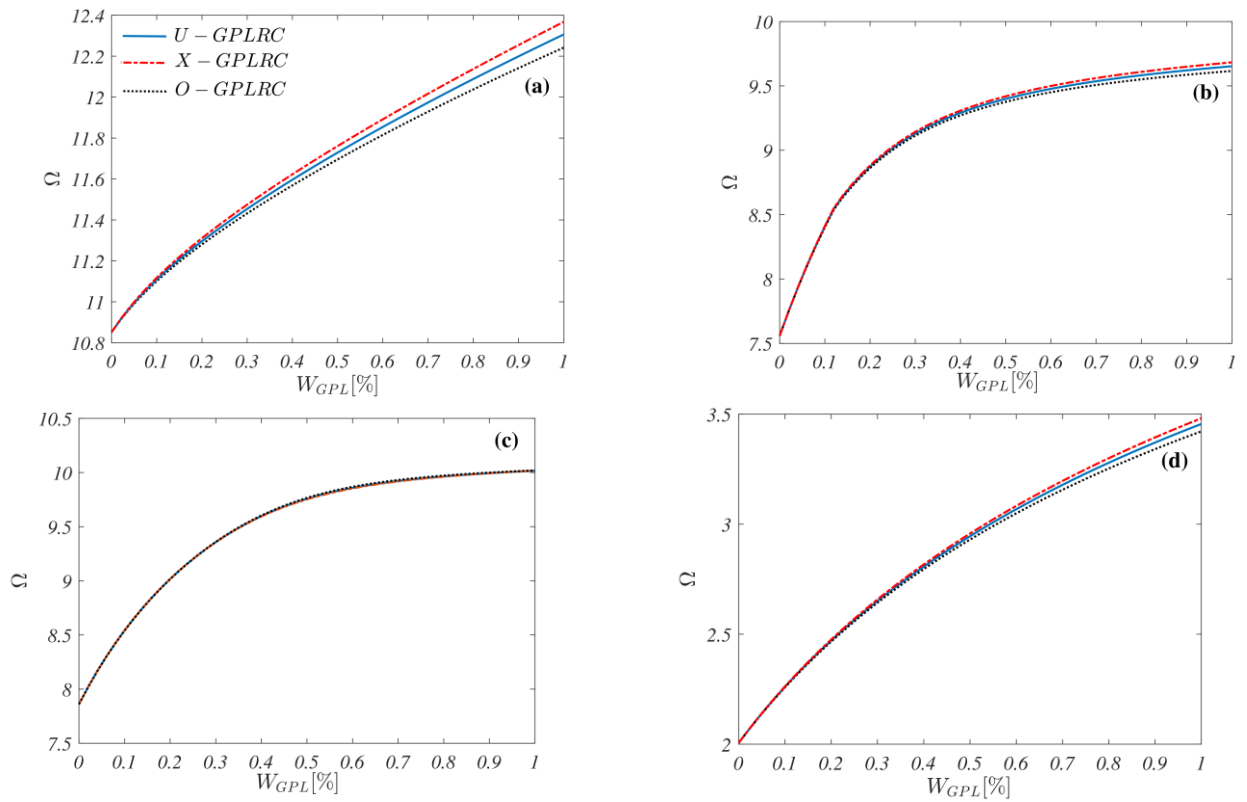


Fig. 5 Fundamental dimensionless frequency of FG-GPLRC conical panel with respect to GPL weight fraction for various types of grading. (a: CCCC, b: CFCF, c: CCFF, d: CFFF)

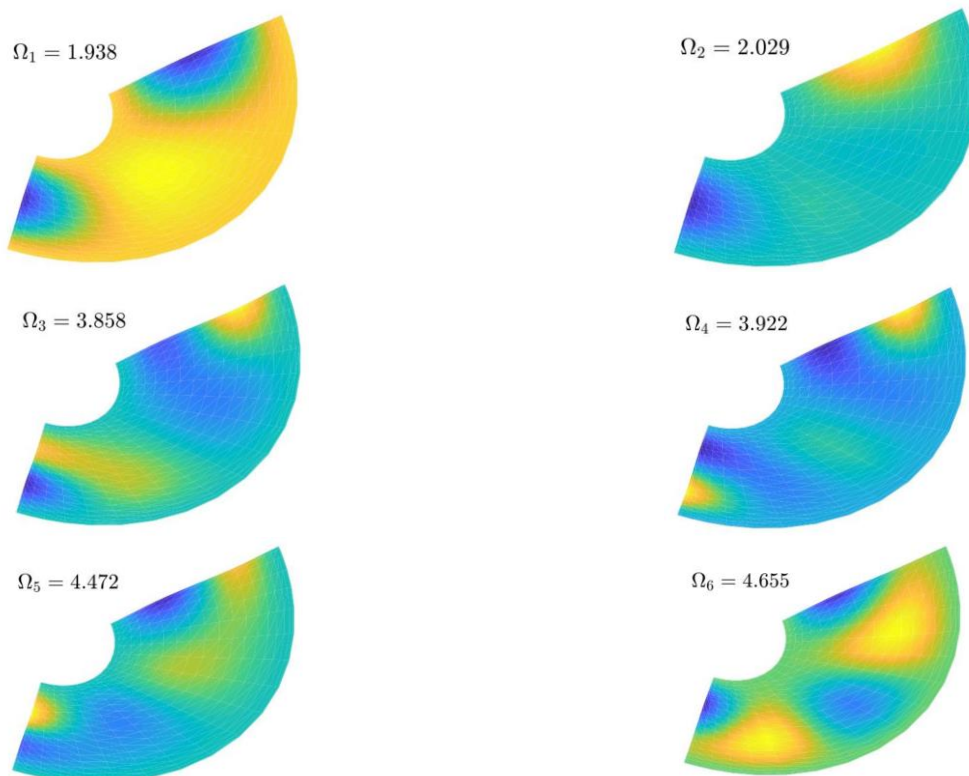


Fig. 6 First six dimensionless frequencies and corresponding mode shapes of X-GPLRC conical panel.

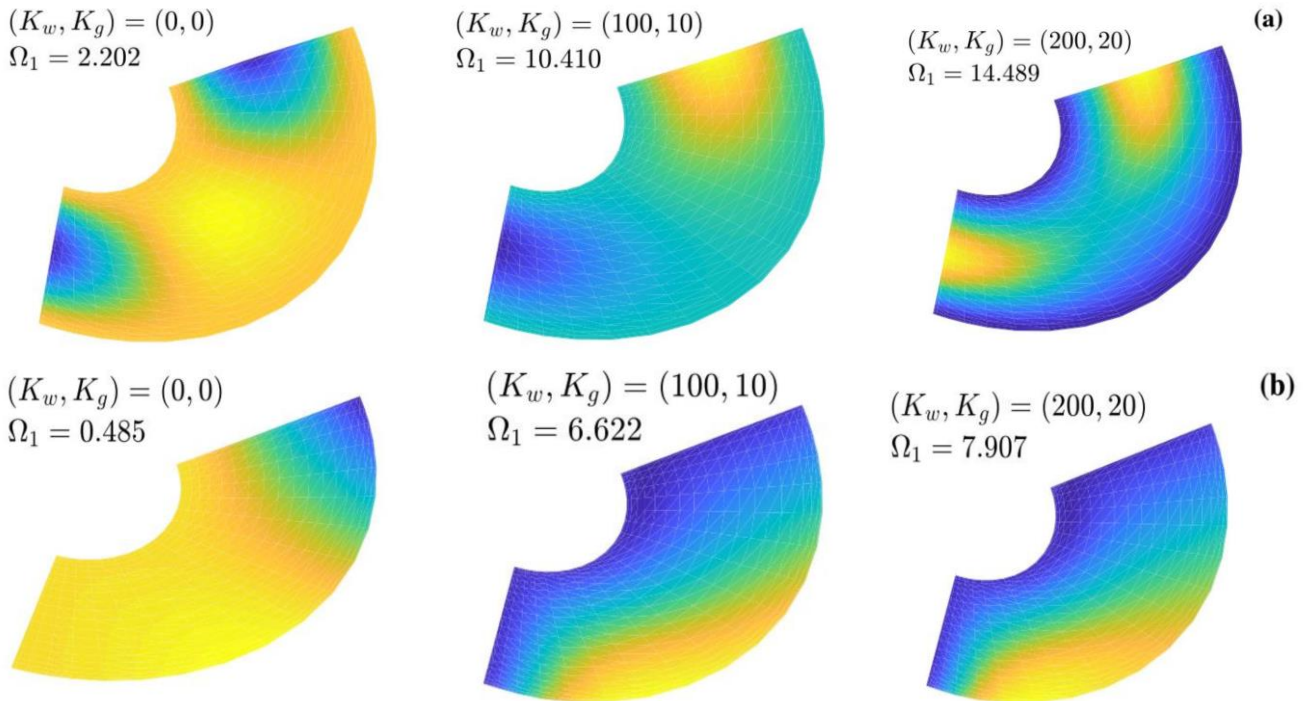


Fig. 7 Fundamental dimensionless frequency and corresponding mode shape of X-GPLRC conical panel for various elastic foundation coefficients. (a: FCFC, b: FFCC)

References

- Affdl, J.H. and Kardos, J.L. (1976), "The HalpinTsai equations: a review", *Polym. Eng. Sci.*, **16**(5), 344-352. <https://doi.org/10.1002/pen.760160512>.
- Akgöz, B. and Civalek, O. (2011), "Nonlinear vibration analysis of laminated plates resting on nonlinear two-parameters elastic foundations", *Steel. Compos. Struct.*, **11**(5), 403-421. <https://doi.org/10.12989/scs.2011.11.5.403>.
- Anirudh, B., Ganapathi, M., Anant, C. and Polit, O. (2019), "A comprehensive analysis of porous graphene-reinforced curved beams by finite element approach using higher-order structural theory: Bending, vibration and buckling", *Compos. Struct.*, **222**, p.110899. <https://doi.org/10.1016/j.compstruct.2019.110899>.
- Bao, S., Wang, S. (2019), "A unified procedure for free transverse vibration of rectangular and annular sectorial plates", *Arch. Appl. Mech.*, **89**(8), 1485-1499. <https://doi.org/10.1007/s00419-019-01519-y>.
- Bardell, N. S., Dunsdon, J. M., and Langley, R. S. (1998), "Free vibration of thin, isotropic, open, conical panels". *J. Sound. Vib.*, **217**(2), 297-320. <https://doi.org/10.1006/jsvi.1998.1761>.
- Cadelano, E., Palla, P.L., Giordano, S. and Colombo, L. (2009), "Nonlinear elasticity of monolayer graphene", *Phys. Rev. Lett.*, **102**(23), 235502. <https://doi.org/10.1103/PhysRevLett.102.235502>.
- Chandra, Y., Chowdhury, R., Scarpa, F., Adhikari, S., Sienz, J., Arnold, C., Murmu, T. and Bould, D. (2012), "Vibration frequency of graphene based composites: a multiscale approach", *Mat. Sci. Eng. B-Adv.*, **177**(3), 303-310. <https://doi.org/10.1016/j.mseb.2011.12.024>.
- Civalek, O. (2006), "Free vibration analysis of composite conical shells using the discrete singular convolution algorithm", *Steel. Compos. Struct.*, **6**(4), 353. <https://doi.org/10.12989/scs.2006.6.4.353>.
- Civalek, O. (2007), "Linear vibration analysis of isotropic conical shells by discrete singular convolution (DSC)", *Struct. Eng. Mech.*, **25**(1), 127-130. <https://doi.org/10.12989/sem.2007.25.1.127>.
- Civalek, O., and Acar, M. H. (2007), "Linear vibration analysis of isotropic conical shells by discrete singular convolution (DSC)", *Int. J. Press. Vessel. Pip.*, **84**(9), 527-535. <https://doi.org/10.1016/j.ijpvp.2007.07.001>.
- Civalek, O. (2008), "Vibration analysis of conical panels using the method of discrete singular convolution", *Commun. Numer. Meth. Eng.*, **24**(3), 169-181. <https://doi.org/10.1002/cnm.961>.
- Civalek, O. (2009), "Fundamental frequency of isotropic and orthotropic rectangular plates with linearly varying thickness by discrete singular convolution method", *Appl. Math. Model.*, **33**(10), 3825-3835. <https://doi.org/10.1016/j.apm.2008.12.019>.
- Dong, Y.H., Zhu, B., Wang, Y., Li, Y.H. and Yang, J. (2018a), "Nonlinear free vibration of graded graphene reinforced cylindrical shells: Effects of spinning motion and axial load", *J. Sound. Vib.*, **437**, 79-96. <https://doi.org/10.1016/j.jsv.2018.08.036>.
- Dong, Y.H., Li, Y.H., Chen, D. and Yang, J. (2018b), "Vibration characteristics of functionally graded graphene reinforced porous nanocomposite cylindrical shells with spinning motion", *Compos. Part. B-Eng.*, **145**, 1-13. <https://doi.org/10.1016/j.compositesb.2018.03.009>.
- Feng, C., Kitipornchai, S. and Yang, J. (2017), "Nonlinear free vibration of functionally graded polymer composite beams reinforced with graphene nanoplatelets (GPLs)", *Eng. Struct.*, **140**, 110-119. <https://doi.org/10.1016/j.engstruct.2017.02.052>.
- Gao, K., Gao, W., Chen, D. and Yang, J. (2018), "Nonlinear free vibration of functionally graded graphene platelets reinforced porous nanocomposite plates resting on elastic foundation", *Compos. Struct.*, **204**, 831-846. <https://doi.org/10.1016/j.compstruct.2018.08.013>.
- Gholami, R. and Ansari, R. (2018), "Nonlinear harmonically excited vibration of third-order shear deformable functionally graded graphene platelet-reinforced composite rectangular plates", *Eng. Struct.*, **156**, 197-209. <https://doi.org/10.1016/j.engstruct.2017.11.019>.
- Gholami, R. and Ansari, R. (2019), "Nonlinear stability and vibration of pre/post-buckled multilayer FG-GPLRPC

- rectangular plates”, *Appl. Math. Model.*, **65**, 627-660. <https://doi.org/10.1016/j.apm.2018.08.038>.
- Guo, H., Cao, S., Yang, T. and Chen, Y. (2018), “Vibration of laminated composite quadrilateral plates reinforced with graphene nanoplatelets using the element-free IMLS-Ritz method”, *Int. J. Mech. Sci.*, **142**, 610-621. <https://doi.org/10.1016/j.ijmecsci.2018.05.029>.
- Javani, M., Kiani, Y., and Eslami, M. R. (2019), “Nonlinear axisymmetric response of temperature-dependent FGM conical shells under rapid heating”, *Acta Mech.*, **230**(9), 3019-3039. <https://doi.org/10.1007/s00707-019-02459-y>.
- Javani, M., Kiani, Y., and Eslami, M. R. (2020), “Thermal buckling of FG graphene platelet reinforced composite annular sector plates”, *Thin. Wall. Struct.*, **148**, p. 106589. <https://doi.org/10.1016/j.tws.2019.106589>.
- Javed, S., Viswanathan, K. K., Aziz, Z. A., and Lee, J. H. (2016), “Vibration analysis of a shear deformed anti-symmetric angle-ply conical shells with varying sinusoidal thickness”, *Struct. Eng. Mech.*, **58**(6), 1001-1020. <https://doi.org/10.12989/sem.2016.58.6.1001>
- Kiani, Y. (2018), “Isogeometric large amplitude free vibration of graphene reinforced laminated plates in thermal environment using NURBS formulation”, *Comput. Method. Appl. M.*, **332**, 86-101. <https://doi.org/10.1016/j.cma.2017.12.015>.
- Kiani, Y., Dimitri, R., and Tornabene, F. (2018), “Free vibration study of composite conical panels reinforced with FG-CNTs”. *Eng. Struct.*, **172**, 472-482. <https://doi.org/10.1016/j.engstruct.2018.06.006>.
- Kiani, Y., And Mirzaei, M. (2019). “Isogeometric thermal postbuckling of FG-GPLRC laminated plates”, *Steel and Compos. Struct.*, **32**(6), 821-832. <https://doi.org/10.12989/scs.2019.32.6.821>.
- Kitipornchai, S., Chen, D. and Yang, J. (2017), “Free vibration and elastic buckling of functionally graded porous beams reinforced by graphene platelets”, *Mater. Design.*, **116**, 656-665. <https://doi.org/10.1016/j.matdes.2016.12.061>.
- Kulkarni, Dhaval D., Ikjun Choi, Srikanth S. Singamaneni, and Vladimir V. Tsukruk. (2010) “Graphene oxide- polyelectrolyte nanomembranes”, *ACS. Nano.*, **4**(8) 4667-4676. <https://doi.org/10.1021/nn101204d>.
- Liu, D., Kitipornchai, S., Chen, W. and Yang, J. (2018), “Three-dimensional buckling and free vibration analyses of initially stressed functionally graded graphene reinforced composite cylindrical shell”, *Compos. Struct.*, **189**, 560-569. <https://doi.org/10.1016/j.compstruct.2018.01.106>.
- Malekzadeh, P., Setoodeh, A.R. and Shojaee, M. (2018), “Vibration of FG-GPLs eccentric annular plates embedded in piezoelectric layers using a transformed differential quadrature method”, *Comput. Method. Appl. M.*, **340**, 451-479. <https://doi.org/10.1016/j.cma.2018.06.006>.
- Novoselov, K.S., Geim, A.K., Morozov, S.V., Jiang, D., Zhang, Y., Dubonos, S.V., Grigorieva, I.V. and Firsov, A.A. (2004), “Electric field effect in atomically thin carbon films”, *Science*, **306**(5696), 666-669. <https://doi.org/10.1126/science.1102896>.
- Potts, J.R., Dreyer, D.R., Bielawski, C.W. and Ruoff, R.S. (2011), “Graphene-based polymer nanocomposites”, *Polymer*, **52**(1), 5-25. <https://doi.org/10.1016/j.polymer.2010.11.042>.
- Rafiee, M.A., Rafiee, J., Wang, Z., Song, H., Yu, Z.Z. and Koratkar, N. (2009), “Enhanced mechanical properties of nanocomposites at low graphene content”, *ACS Nano.*, **3**(12), 3884-3890. <https://doi.org/10.1021/nn9010472>.
- Rahmani, M., Mohammadi, Y., & Kakavand, F. (2019), “Vibration analysis of sandwich truncated conical shells with porous FG face sheets in various thermal surroundings”, *Steel. Compos. Struct.*, **32**(2), 239-252. <https://doi.org/10.12989/scs.2019.32.2.239>.
- Reddy, C.D., Rajendran, S. and Liew, K.M. (2006), “Equilibrium configuration and continuum elastic properties of finite sized graphene”, *Nanotechnology*, **17**(3), p.864. <https://doi.org/10.1088/0957-4484/17/3/042>.
- Reddy, J.N., (2006), *Theory and analysis of elastic plates and shells*, CRC press.
- Saidi, A.R., Bahaadini, R. and Majidi-Mozafari, K. (2019), “On vibration and stability analysis of porous plates reinforced by graphene platelets under aerodynamical loading”, *Compos. Part. B-Eng.*, **164**, 778-799. <https://doi.org/10.1016/j.compositesb.2019.01.074>.
- Scarpa, F., Adhikari, S. and Phani, A.S. (2009), “Effective elastic mechanical properties of single layer graphene sheets”, *Nanotechnology*, **20**(6), p.065709.
- Shen, H.S., Lin, F. and Xiang, Y. (2017a), “Nonlinear vibration of functionally graded graphene-reinforced composite laminated beams resting on elastic foundations in thermal environments”, *Nonlinear. Dynam.*, **90**(2), 899-914. <https://doi.org/10.1007/s11071-017-3701-0>.
- Shen, H.S., Xiang, Y. and Lin, F. (2017b), “Nonlinear vibration of functionally graded graphene-reinforced composite laminated plates in thermal environments”, *Comput. Method. Appl. M.*, **319**, 175-193. <https://doi.org/10.1016/j.cma.2017.02.029>.
- Shen, H.S., Xiang, Y. and Fan, Y. (2017c), “Nonlinear vibration of functionally graded graphene-reinforced composite laminated cylindrical shells in thermal environments”, *Compos. Struct.*, **182**, 447-456. <https://doi.org/10.1016/j.compstruct.2017.09.010>.
- Shen, H.S., Xiang, Y., Fan, Y. and Hui, D. (2018), “Nonlinear vibration of functionally graded graphene-reinforced composite laminated cylindrical panels resting on elastic foundations in thermal environments”, *Compos. Part. B-Eng.*, **136**, 177-186. <https://doi.org/10.1016/j.compositesb.2017.10.032>.
- Shen, H.S., Xiang, Y. and Fan, Y. (2019a), “Nonlinear vibration of thermally postbuckled FG-GRC laminated beams resting on elastic foundations”, *Int. J. Struct. Stab. Dy.*, **25**(9), 1507-1520. <https://doi.org/10.1142/S0219455419500512>.
- Shen, H.S., Xiang, Y. and Fan, Y. (2019b), “Vibration of thermally postbuckled FG-GRC laminated plates resting on elastic foundations”, *J. Vib. Control.*, **19**(6), p.1950051. <https://doi.org/10.1177/1077546319825671>.
- Shi, D.Y., Wang, Q.S., Shi, X.J., Pang, F.Z. (2015), “A series solution for the in-plane vibration analysis of orthotropic rectangular plates with non-uniform elastic boundary constraints and internal line supports”, *Arch. Appl. Mech.*, **81**(1), 51-73. <https://doi.org/10.1007/s00419-014-0899-x>
- Song, M., Kitipornchai, S. and Yang J., (2017), “Free and forced vibrations of functionally graded polymer composite plates reinforced with graphene nanoplatelets”, *Compos. Struct.*, **159**, 579-588. <https://doi.org/10.1016/j.compstruct.2016.09.070>.
- Stankovich, S., Dikin, D.A., Dommett, G.H., Kohlhaas, K.M., Zimney, E.J., Stach, E.A., Piner, R.D., Nguyen, S.T. and Ruoff, R.S. (2006), “Graphene-based composite materials”, *Nature*, **442**(7100), p.282. <https://doi.org/10.1038/nature04969>
- Tornabene, F., Viola, E., & Inman, D. J. (2009), “2-D differential quadrature solution for vibration analysis of functionally graded conical, cylindrical shell and annular plate structures”, *J. Sound. Vib.*, **328**(3), 259-290. <https://doi.org/10.1016/j.jsv.2009.07.031>.
- Wang, M., Xu, Y.G., Qiao, P. and Li, Z.M. (2019a), “A two-dimensional elasticity model for bending and free vibration analysis of laminated graphene-reinforced composite beams”, *Compos. Struct.*, **211**, 364-375. <https://doi.org/10.1016/j.compstruct.2018.12.033>.
- Wang, Y., Xie, K., Fu, T. and Shi, C. (2019b), “Vibration response of a functionally graded graphene nanoplatelet reinforced composite beam under two successive moving masses”, *Compos. Struct.*, **209**, 928-939. <https://doi.org/10.1016/j.compstruct.2018.11.014>.
- Wang, A., Chen, H., Hao, Y. and Zhang, W. (2018), “Vibration and bending behavior of functionally graded nanocomposite doubly-curved shallow shells reinforced by graphene nanoplatelets”,

- Results. Phys.*, **9**, 550-559.
<https://doi.org/10.1016/j.rinp.2018.02.062>.
- Wu, H., Kitipornchai, S. and Yang, J. (2017), "Thermal buckling and postbuckling of functionally graded graphene nanocomposite plates", *Mater. Design.*, **132**, 430-441.
<https://doi.org/10.1016/j.matdes.2017.07.025>.
- Zhang, Y.Y., Wang, C.M., Cheng, Y. and Xiang, Y. (2011), "Mechanical properties of bilayer graphene sheets coupled by sp³ bonding", *Carbon*, **49**(13), 4511-4517.
<https://doi.org/10.1016/j.carbon.2011.06.058>.
- Zhao, X., Zhang, Q., Chen, D. and Lu, P. (2010), "Enhanced mechanical properties of graphene-based poly (vinyl alcohol) composites", *Macromolecules*, **43**(5), 2357-2363.
<https://doi.org/10.1021/ma902862u>.
- Zhao, Z., Feng, C., Wang, Y. and Yang, J. (2017), "Bending and vibration analysis of functionally graded trapezoidal nanocomposite plates reinforced with graphene nanoplatelets (GPLs)", *Compos. Struct.*, **180**, 799-808.
<https://doi.org/10.1016/j.compstruct.2017.08.044>.